

Crystallization behavior and IR structure of yttrium aluminosilicate glasses

ZHENG, Q., LIU, Y., LI, M., LIU, Z., HU, Y., ZHANG, X., DENG, Wei and WANG, M.

Available from Sheffield Hallam University Research Archive (SHURA) at:

<http://shura.shu.ac.uk/25311/>

This document is the author deposited version. You are advised to consult the publisher's version if you wish to cite from it.

Published version

ZHENG, Q., LIU, Y., LI, M., LIU, Z., HU, Y., ZHANG, X., DENG, Wei and WANG, M. (2019). Crystallization behavior and IR structure of yttrium aluminosilicate glasses. *Journal of the European Ceramic Society*.

Copyright and re-use policy

See <http://shura.shu.ac.uk/information.html>

1
2 **Crystallization behavior and IR structure of yttrium aluminosilicate**
3
4
5 **glasses**

6
7 Qingshuang Zheng^{1,2}, Yucheng Liu^{1,2}, Mei Li^{1,2,3*}, Zhaogang Liu^{2,3}, Yanhong Hu^{2,3},
8
9
10 Xiaowei Zhang^{1,2,3}, Wei Deng⁴, Mitang Wang^{1,2,3*}
11

12
13 (1 School of Materials Science and Engineering, University of Shanghai for Science and
14
15
16 Technology, Shanghai 200093, China;
17

18
19 2 School of Material and Metallurgy, Inner Mongolia University of Science and
20
21
22 Technology, Baotou 014010, China;
23

24
25 3 Key Laboratory of Green Extraction & Efficient Utilization of Light Rare-Earth
26
27
28 Resources, Ministry of Education, Baotou 014010, China;
29

30
31 4 Materials and Engineering Research Institute, Sheffield Hallam University, Sheffield
32
33
34 S1 1WB, UK)
35

36 **Abstract:** The crystallization of four Y₂O₃-Al₂O₃-SiO₂ (YAS) glasses were investigated
37
38 to prepare YAS glass ceramics precipitated singly/mainly Y₂Si₂O₇ or Y_{4.67}(SiO₄)₃O
39
40 apatite, and to explore the crystallization difference between the stoichiometric parent
41
42 glass (SPG) and non-stoichiometric parent glass (NSPG). The DSC results revealed that
43
44 glass locating at the higher liquidus surface temperature has lower crystallization peak
45
46 temperature, which indicating that the corresponding glass has higher crystallization
47
48 potential to crystallize easily. Crystallization of the NSPG samples is along surface and
49
50 caused by phase separation, while SPG sample is the surface crystallization at the first
51
52
53
54
55
56
57
58
59
60
61
62
63
64
65

1
2 exothermic peak temperature and overall crystallization at the second exothermic peak
3
4
5 temperature. Glass ceramics only containing γ - $\text{Y}_2\text{Si}_2\text{O}_7$ or $\text{Y}_{4.67}(\text{SiO}_4)_3\text{O}$ apatite are
6
7 obtained successfully, and which are illustrated by fitting FTIR spectra. These results
8
9
10 can provide technical guide for controlling the crystallization process and the types of
11
12 precipitated crystals in YAS glass for different application potentials.
13
14

15
16 **Keywords:** Crystallization; Y_2O_3 ; Glass ceramics; Structure
17

18 19 **1. Introduction** 20

21
22 Yttrium aluminosilicate (YAS) glass and glass ceramics have attracted much
23
24 attention due to their numerous excellent properties [1-8]. The low thermal expansion
25
26 coefficients (TECs) makes YAS glasses promising for application as adhesives for
27
28 joining, especially for the non-oxide ceramics such as SiC and Si_3N_4 [3,4]. YAS system
29
30 glass has interesting chemical durability [5,6], so the glass can prepare glass
31
32 microspheres (including Yttrium-89) used to treat cancers [6,7]. YAS glasses and glass
33
34 ceramics can accommodate high concentration of rare earth ions and have great
35
36 potential for optical applications [8]. YAS glasses are also used in optical fibers and
37
38 corresponding glass ceramics can be used as a matrix for storage of long-lived actinides
39
40 [9-11].
41
42
43
44
45
46
47
48
49

50
51 Types of crystal precipitated have great influence on the properties of glass
52
53 ceramics, thereby it is essential to explore clearly the crystallization of YAS glass. The
54
55 YAS glass-forming zone includes $\text{Y}_2\text{Si}_2\text{O}_7$, SiO_2 , mullite and Al_2O_3 phase region in the
56
57
58
59
60
61
62
63
64
65

1
2 $Y_2O_3-Al_2O_3-SiO_2$ phase diagram [9, 12]. Najim Sadiki et al. [9] studied four
3
4
5 compositions of YAS glass melted by a laboratory-scale solar furnace, they found that
6
7
8 mullite, SiO_2 , $\gamma-Y_2Si_2O_7$ and a little $\beta-Y_2Si_2O_7$ can be crystallized in studied glass, but
9
10
11 two or three crystals were precipitated finally from each glass for these compositions. S.
12
13 Ahmadet al. [13] found unknown phase for YAS glass ceramic during high temperature
14
15
16 long heat treatments, and the chemical composition of the unknown phase is determined
17
18
19 to be Y = 8.45, Si = 16.45, Al = 12.82 and O = 62.26 (at. %). Yttrium silicates, including
20
21
22 $Y_2Si_2O_7$, Y_2SiO_5 and $Y_{4.67}(SiO_4)_3O$ apatite, have many potential applications such as
23
24
25 high-temperature structural ceramics, oxidation protective coatings and environmental
26
27
28 barrier coatings, because of their specific mechanical, thermal, tribological and
29
30
31 dielectric properties and environmental durability [14]. YAS glass ceramics are superior
32
33
34 than YAS glasses in mechanical performance and oxidation resistance when they are
35
36
37 used as sintering additives for preparing SiC ceramic or Si_3N_4 ceramic [15]. Matching
38
39
40 TECs of the joined components and filler is essential for minimizing the thermal
41
42
43 stresses in the joint, so that the thermal expansion coefficients of sintering additives or
44
45
46 filler should be in the same range or lower than those of the ceramic materials to be
47
48
49 joined [3]. As the sintering additives or filler, the TEC of YAS glass ceramics depends
50
51
52 on the all components including precipitated crystal types and contents, as well as
53
54
55 residual glass content and compositions. It is well known that the thermal expansion
56
57
58 coefficient of $Y_2Si_2O_7$ is smaller than other kind of crystals precipitated in YAS glass
59
60
61
62
63
64
65

1 ceramics and hence $Y_2Si_2O_7$ phase would be in the best interest for YAS glass filler with
2
3
4 lower TEC. Besides, apatite-type rare earth silicates have been found to have the low
5
6
7 activation energy in the ionic conduction, and thus it is suitable for an
8
9
10 intermediate-temperature solid oxide fuel cells (SOFC) electrolyte [16]. Recently, Liao
11
12
13 T et al. [17] investigated the position preference and diffusion mechanisms of interstitial
14
15
16 oxygen ions in lanthanum silicate $La_{9.33}Si_6O_{26}$ using density functional theory. For the
17
18
19 yttrium silicate ($Y_{4.67}(SiO_4)_3O$ apatite), it can be prepared by hydrothermal method,
20
21
22 solid-state reaction method, solid-liquid reaction method and so on. However, these
23
24
25 methods need tens to hundreds of hours and high cost. Glass crystallization might be
26
27
28 another effective way to prepare $Y_{4.67}(SiO_4)_3O$ apatite, but until now there are no reports
29
30
31 about the glass ceramics containing $Y_{4.67}(SiO_4)_3O$ apatite.

32
33
34 From the above, many researchers studied the crystallization of the YAS glass
35
36
37 system but $Y_{4.67}(SiO_4)_3O$ apatite has not been found and $Y_2Si_2O_7$ is not as single
38
39
40 crystalline phase to precipitate in the YAS glass ceramics. In this work, the
41
42
43 crystallization behavior of YAS parent glasses with different chemical compositions that
44
45
46 were elected according to $Y_2O_3-Al_2O_3-SiO_2$ phase diagram have been studied in order to
47
48
49 prepare YAS glass ceramics precipitated singly/mainly $Y_2Si_2O_7$ or $Y_{4.67}(SiO_4)_3O$ apatite
50
51
52 crystal. Besides, the crystallization behavior of stoichiometric parent glass (SPG)
53
54
55 having the same stoichiometric ratio with the precipitated crystal and
56
57
58 non-stoichiometric parent glass (NSPG) is also investigated and compared in details.
59
60
61
62
63
64
65

2. Experimental

The glasses were prepared by using the following reagent grade materials, Y_2O_3 (99.9 %), Al_2O_3 (99.9 %), SiO_2 (99.0 %). Table 1 shows the chemical composition of the glasses. According to the Y_2O_3 - Al_2O_3 - SiO_2 phase diagram (Fig. 1) [12], the chemical compositions of glasses were chosen and named after Y, Y2S, M and YMS. In order to make glass precipitate singly/mainly $\text{Y}_2\text{Si}_2\text{O}_7$ crystal, the Y glass chemical composition was designed to be located in the $\text{Y}_2\text{Si}_2\text{O}_7$ phase region of Y_2O_3 - Al_2O_3 - SiO_2 phase diagram. The M sample is located in the mullite phase region and the YMS sample is located in the triple eutectic point. The Y sample is elected regarding as standard sample to study the influence of SPG and NSPG on crystallization behavior, because the Y glass ceramic was observed to have only single crystallized phase $\text{Y}_2\text{Si}_2\text{O}_7$ by crystal analysis. Therefore, the SPG (named Y2S) was selected according to a certain molar ratio ($\text{Y}_2\text{O}_3:\text{SiO}_2 = 1:2$) that was the same with the stoichiometric ratio of $\text{Y}_2\text{Si}_2\text{O}_7$. The ratio is shown in red line in Fig. 1. Besides the certain molar ratio, the Y2S is also determined according to two other requirements. First, the composition can melt into glass by melting at high temperature and cooling at room temperature. Second, the composition should be as close to the Y sample composition as possible so that avoid large crystallization difference caused by component deviation. After multiple experiments, the chemical composition of Y2S sample is identified as $25\text{Y}_2\text{O}_3$ - $25\text{Al}_2\text{O}_3$ - 50SiO_2 (mol%).

1
2 A mixture of the precursor oxide powders (400 g) was mixed in mortar and melted
3
4 in platinum crucible. The raw materials according to the calculated weight were mixed
5
6 evenly and ground uniform, then melted at 1550 °C for 3 h. The melt was cast into a
7
8 preheated graphite mould and then annealed at glass transition temperature for 2 h to
9
10 eliminate the residual stress in glass structure. The X-ray fluorescence was used to
11
12 check the resulting glasses chemical composition, and the results agreed with the
13
14 experimental error of ± 3 % with the compositions of the initial batches. The amorphous
15
16 character of samples was confirmed by X-ray diffraction. The annealed glasses are
17
18 controlled to crystallize by two-step heat treatment. The glasses were heated firstly at
19
20 5 °C/min to nucleation temperature, held for 1 h, and then heated again at 5 °C/min to
21
22 crystallization temperature and held for 2.5 h, finally cooled down to room temperature
23
24 by natural cooling. The nucleation and crystallization temperature are determined to be
25
26 about 20 °C above glass transition temperature (T_g) and crystallization peak
27
28 temperature (T_c).
29
30
31
32
33
34
35
36
37
38
39
40
41

42 T_g and T_c are obtained to draw up the heat treatment schedule by the differential
43
44 scanning calorimetry (DSC, NETZSCH DSC STA449C). 15 mg of glass powder
45
46 (particle size of about 80 μm) in an alumina crucible was heated from room temperature
47
48 to 1400 °C at the heating rate of 10 K/min. In order to study the crystallization of
49
50 glasses with different chemical compositions, the glasses were cut into strips (5×5×10
51
52 mm) then controlled to crystallize by two-step heat treatment. The crystal phases
53
54
55
56
57
58
59
60
61
62
63
64
65

1 precipitated were analyzed by X-ray diffractometer (Rigaku XRD Miniflex600) for
2
3
4 powdered glass ceramic in 10-80 ° angle range at scanning speed of 4 °/min. In order to
5
6
7 excellently study the microstructure, the glass ceramic was polished and its surface was
8
9
10 corroded by 4 wt% HF for 30 s at room temperature to observe the microstructure by a
11
12
13 scanning electron microscopy (FEI SEM QUANTA400), and prior to characterization
14
15
16 all samples were sputtered with gold by using a sputtering machine.
17
18

19 In order to study the relation of glass structure and crystallization behavior, the
20
21 parent glass was detected by a Fourier transform infrared spectrometer (Shimadzu
22
23 FT-IR Prestige-21) to measure the infrared absorption spectra in the wavenumber range
24
25 of 400-4000 cm^{-1} with 2 cm^{-1} resolution, the transmission technique was applied and the
26
27 samples were prepared as KBr pellets. The IR data were processed by normalization to
28
29
30 eliminate the effect of uneven sample thickness during preparing.
31
32
33
34
35

36 **3. Results and discussion**

37 **3.1. Thermal analysis**

38
39 Fig. 2 shows the DSC results of four samples including endothermic and
40
41 exothermic peak at a heating rate of 10 K/min. Glass transition temperature was
42
43 standardized by calculating the inflection point nearby endothermic peak with the
44
45 second derivative method. The temperature at the inflection point was defined as the
46
47 glass transition temperature. The glass transition temperature (T_g) of Y, Y2S, M and
48
49
50
51
52
53
54
55
56
57
58
59
60
61
62
63
64
65
66
67
68
69
70
71
72
73
74
75
76
77
78
79
80
81
82
83
84
85
86
87
88
89
90
91
92
93
94
95
96
97
98
99
100
101
102
103
104
105
106
107
108
109
110
111
112
113
114
115
116
117
118
119
120
121
122
123
124
125
126
127
128
129
130
131
132
133
134
135
136
137
138
139
140
141
142
143
144
145
146
147
148
149
150
151
152
153
154
155
156
157
158
159
160
161
162
163
164
165
166
167
168
169
170
171
172
173
174
175
176
177
178
179
180
181
182
183
184
185
186
187
188
189
190
191
192
193
194
195
196
197
198
199
200
201
202
203
204
205
206
207
208
209
210
211
212
213
214
215
216
217
218
219
220
221
222
223
224
225
226
227
228
229
230
231
232
233
234
235
236
237
238
239
240
241
242
243
244
245
246
247
248
249
250
251
252
253
254
255
256
257
258
259
260
261
262
263
264
265
266
267
268
269
270
271
272
273
274
275
276
277
278
279
280
281
282
283
284
285
286
287
288
289
290
291
292
293
294
295
296
297
298
299
300
301
302
303
304
305
306
307
308
309
310
311
312
313
314
315
316
317
318
319
320
321
322
323
324
325
326
327
328
329
330
331
332
333
334
335
336
337
338
339
340
341
342
343
344
345
346
347
348
349
350
351
352
353
354
355
356
357
358
359
360
361
362
363
364
365
366
367
368
369
370
371
372
373
374
375
376
377
378
379
380
381
382
383
384
385
386
387
388
389
390
391
392
393
394
395
396
397
398
399
400
401
402
403
404
405
406
407
408
409
410
411
412
413
414
415
416
417
418
419
420
421
422
423
424
425
426
427
428
429
430
431
432
433
434
435
436
437
438
439
440
441
442
443
444
445
446
447
448
449
450
451
452
453
454
455
456
457
458
459
460
461
462
463
464
465
466
467
468
469
470
471
472
473
474
475
476
477
478
479
480
481
482
483
484
485
486
487
488
489
490
491
492
493
494
495
496
497
498
499
500
501
502
503
504
505
506
507
508
509
510
511
512
513
514
515
516
517
518
519
520
521
522
523
524
525
526
527
528
529
530
531
532
533
534
535
536
537
538
539
540
541
542
543
544
545
546
547
548
549
550
551
552
553
554
555
556
557
558
559
560
561
562
563
564
565
566
567
568
569
570
571
572
573
574
575
576
577
578
579
580
581
582
583
584
585
586
587
588
589
590
591
592
593
594
595
596
597
598
599
600
601
602
603
604
605
606
607
608
609
610
611
612
613
614
615
616
617
618
619
620
621
622
623
624
625
626
627
628
629
630
631
632
633
634
635
636
637
638
639
640
641
642
643
644
645
646
647
648
649
650
651
652
653
654
655
656
657
658
659
660
661
662
663
664
665
666
667
668
669
670
671
672
673
674
675
676
677
678
679
680
681
682
683
684
685
686
687
688
689
690
691
692
693
694
695
696
697
698
699
700
701
702
703
704
705
706
707
708
709
710
711
712
713
714
715
716
717
718
719
720
721
722
723
724
725
726
727
728
729
730
731
732
733
734
735
736
737
738
739
740
741
742
743
744
745
746
747
748
749
750
751
752
753
754
755
756
757
758
759
760
761
762
763
764
765
766
767
768
769
770
771
772
773
774
775
776
777
778
779
780
781
782
783
784
785
786
787
788
789
790
791
792
793
794
795
796
797
798
799
800
801
802
803
804
805
806
807
808
809
810
811
812
813
814
815
816
817
818
819
820
821
822
823
824
825
826
827
828
829
830
831
832
833
834
835
836
837
838
839
840
841
842
843
844
845
846
847
848
849
850
851
852
853
854
855
856
857
858
859
860
861
862
863
864
865
866
867
868
869
870
871
872
873
874
875
876
877
878
879
880
881
882
883
884
885
886
887
888
889
890
891
892
893
894
895
896
897
898
899
900
901
902
903
904
905
906
907
908
909
910
911
912
913
914
915
916
917
918
919
920
921
922
923
924
925
926
927
928
929
930
931
932
933
934
935
936
937
938
939
940
941
942
943
944
945
946
947
948
949
950
951
952
953
954
955
956
957
958
959
960
961
962
963
964
965
966
967
968
969
970
971
972
973
974
975
976
977
978
979
980
981
982
983
984
985
986
987
988
989
990
991
992
993
994
995
996
997
998
999
1000

1
2 more non-bridging oxygens (NBOs) in the glassy structure [18,19]. Through the
3
4 difference of T_g , it can be known that Y and Y2S glasses have more non-bridging
5
6 oxygen than M and YMS glasses. The crystallization peak temperature (T_c) of Y, Y2S,
7
8 M and YMS glass are 1137 °C, 1112 °C, 1191 °C and 1253 °C respectively, it can be
9
10 also observed that Y2S glass has two crystallization peaks at 1112 °C (T_c) and 1344 °C
11
12 (T_{c2}). More interesting, except Y2S glass, there is a small exothermic peak for other
13
14 glasses (named T_x) between T_g and T_c in DSC curve. This small exothermic peak might
15
16 be caused by the phase separation of glass during heating process, which will be
17
18 described in next section. The T_x of Y, M and YMS glasses are 1035 °C, 999 °C and
19
20 1015 °C, respectively. The values of T_g , T_x , T_c and T_{c2} for all glasses are summarized
21
22 in table 1, and there is an error of ± 1 °C for T_g and T_c .
23
24
25
26
27
28
29
30
31
32

33
34 By comparing glass crystallization peak temperatures (T_c : YMS>M>Y>Y2S) with
35
36 the temperatures of the liquidus surface (T_s : Y2S>Y>M>YMS) obtained from phase
37
38 diagram of the Y_2O_3 - Al_2O_3 - SiO_2 system with plots of the isotherms [20], one can
39
40 observe an interesting fact that the higher T_s of glass chemical composition locating at
41
42 phase diagram of the Y_2O_3 - Al_2O_3 - SiO_2 system, the lower T_c of corresponding glass.
43
44
45 With the same chemical composition, the glass obtained at a slower cooling rate would
46
47 have a lower enthalpy than that obtained using a faster cooling rate [21]. Hence, the
48
49 faster cooling glass possesses higher enthalpy in glass structure and has better
50
51 crystallization potential, thereby it can be more easily crystallized and consequently
52
53
54
55
56
57
58
59
60
61
62
63
64
65

1 exhibits lower T_c . In this work, the experiment adopts identical cooling rate, so the
2
3
4 chemical composition is the single factor influencing the enthalpy of glass. The glass
5
6
7 chemical composition locating at higher T_s may have a higher enthalpy in glass
8
9
10 structure and hence its T_c is lower, as a result, corresponding glass obtained at same
11
12
13 cooling rate is crystallized more easily.
14

15 **3.2. Crystallization**

16
17
18
19 Generally, the nucleation temperature for preparing glass ceramics is above $50\text{ }^\circ\text{C}$
20
21
22 glass transition temperature. In this work the nucleation temperature of all samples is set
23
24
25 as $920\text{ }^\circ\text{C}$ for simplicity and then the samples are heat treated at different T_x and T_c . Fig.
26
27
28 3 shows XRD patterns of glasses heat treated according to the heat treatment schedule
29
30
31 listed in Table 2. As shown in Fig. 3(a), XRD patterns of Y-1, M-1 and YMS-1 samples
32
33
34 heat treated at $920\text{ }^\circ\text{C}$ for 2 h and their T_x temperature for 2.5 h are diffuse X-ray peak,
35
36
37 showing that they still keep glassy nature and there are no precipitated crystals in
38
39
40 glasses after heat treated at nucleation temperature and T_x temperature. Fig. 4 gives the
41
42
43 SEM photograph for the heat treated glasses. After heat treatment at $920\text{ }^\circ\text{C}$ for 1 h and
44
45
46 $1035\text{ }^\circ\text{C}$ for 2.5 h, there are some ununiform circular area in Y-1 sample as shown in Fig.
47
48
49 4(a), presumably phase separation is occurred for Y-1 sample combining with no crystal
50
51
52 precipitated as shown in Fig. 3(a). Similarly, the phase separation might be occurred in
53
54
55 M-1 and YMS-1 samples. Thereby, it can be considered that the exothermic peak for Y,
56
57
58 M and YMS glasses between glass transition temperature and crystallization peak
59
60
61
62
63
64
65

1
2 temperature could be attributed to occurrence of phase separation of glass sample during
3
4
5 heat process.
6

7
8 After heat treatment at 920 °C for 1 h and 1137 °C (crystallization peak
9
10 temperature) for 2.5 h, the γ -Y₂Si₂O₇ crystal is precipitated in Y-2 sample as shown in
11
12 Fig. 3 (b). Unfortunately, a little diffraction peaks at 25.95 °, 31.12 °, 35.37 ° and
13
14 40.91 ° in Y-2 sample appear and are not attributable, but the precipitated crystals in Y-2
15
16 sample are mainly the γ -Y₂Si₂O₇. Comparing the phase separation regions occurred in
17
18 Y-1 sample (Fig. 4(a)) with the circular regions of crystal precipitated in Y-2 sample
19
20 (Fig. 4(b)), they are similar in shape. After the same heat treatment time (2.5 h) at
21
22 different temperature (Tx=1035 °C and Tc=1137 °C), the size of the crystal area in Y-2
23
24 sample is somewhat larger than the size of the phase separation area in Y-1 sample due
25
26 to the crystal growth at higher temperature (1137 °C for Y-2 and 1035 °C for Y-1), and
27
28 the phase separation area is about 7.4 μm (Fig. 4(a), line 1) and 9.6 μm for crystal area
29
30 (Fig. 4(b), line 2) respectively. Apart from similar shape, the content of Si and Y
31
32 elements in phase separation area is higher than that near phase separation region (as
33
34 shown in Fig. 5), the content of Si and Y elements in phase separation area is enriched
35
36 as formation of phase separation, the content of Si and Y elements are 25.86 and 13.10
37
38 (At%) nearby the phase separation region, after occurrence of phase separation they are
39
40 accumulated to 28.94 and 16.21 (At%) respectively in the phase separation area.
41
42
43
44
45
46
47
48
49
50
51
52
53
54
55
56
57 Aggregation of Si and Y elements in some small areas serves nucleation and crystal
58
59
60
61
62
63
64
65

1 growth of corresponding crystal such as $Y_2Si_2O_7$ crystal. Therefore, it can be concluded
2
3
4 that the crystallization mechanism of Y glass heat treated at 920 °C for 1 h and 1137 °C
5
6
7 for 2.5 h is caused by phase separation occurred at lower temperature, and phase
8
9
10 separation provides a beneficial condition for crystallization.
11

12
13 As for M and YMS samples, after heat treating at 920 °C for 1 h and their
14
15
16 crystallization peak temperature (1191 °C and 1253 °C) for 2.5 h respectively,
17
18
19 comparing M-1 with M-2 and YMS-1 with YMS-2 samples, it can be found that M-2
20
21
22 and YMS-2 samples are crystallized at their surface, and they have identical crystal
23
24
25 phases including γ - $Y_2Si_2O_7$, mullite and cristobalite (Fig. 3 (c)), it is reasonable to
26
27
28 conclude that the phase separation occurred also in M and YMS glasses similarly which
29
30
31 provides beneficial condition for crystallization of corresponding crystals, while the
32
33
34 crystal growth rate for M and YMS is not the same according to their different surface
35
36
37 crystalline thickness (Fig. 6 (e) and (f)), the surface crystalline thickness of M-2 glass
38
39
40 ceramic is much smaller than YMS-2, suggesting the crystallization rate of YMS glass
41
42
43 is much larger than M glass. YMS-3 sample annealed at 920 °C for 1 h and 1253 °C for
44
45
46 0.5 h is also shown in Fig. 6 (g), to compare with YMS-2 glass ceramic obtained at
47
48
49 920 °C for 1 h and 1253 °C for 2.5 h, it is really clear that crystallization of YMS is
50
51
52 along sample surface and the crystal growth rate is very fast.
53

54
55
56 Chemical composition of Y2S sample has the same stoichiometric ratio ($Y_2O_3:SiO_2$
57
58
59 = 1:2) with the crystal phase $Y_2Si_2O_7$, it has two crystallization peaks at 1112 °C and
60
61
62
63
64
65

1
2 1344 °C as listed in Table1, thereby Y2S glass is heat treated at 1112 °C and 1344 °C
3
4
5 respectively. Y2S-1 glass ceramic heat treated at 920 °C for 1 h and 1112 °C for 2.5 h is
6
7 observed to crystallize only $Y_{4.67}(SiO_4)_3O$ crystal (Fig. 3(b)), Y2S-2 glass ceramic heat
8
9 treated at 920 °C for 1h and 1344 °C for 2.5 h is observed to crystallize γ - $Y_2Si_2O_7$ and
10
11 little $Y_{4.67}(SiO_4)_3O$ crystal (Fig. 3(b)), formation of the little $Y_{4.67}(SiO_4)_3O$ may be
12
13 occurred around 1112 °C during the sample is heated to 1344 °C. Fig. 4(c) and (d) show
14
15 the SEM images of the Y2S-1 and Y2S-2 glass ceramics respectively, their
16
17 microstructures of crystals precipitated in glass ceramics are really different from the
18
19 crystal microstructure in Y-2 glass ceramic. Obviously, no phase separation exothermic
20
21 peaks in thermal analysis are found in the Y2S glass (Fig. 2), so the crystallization
22
23 mechanism of Y2S glass is different from Y glass. Fig. 6 gives the profile photos of the
24
25 heat treated glasses, it can be found that the Y-2 sample began to crystallize along its
26
27 surface and then crystals grow inwards the sample (Fig. 6 (a)), and Y2S-1 sample has
28
29 the same crystallization way with Y-2 sample (Fig. 6 (b)), however, Y2S-2 sample
30
31 shows overall crystallization process (Fig. 6 (c)) when Y2S glass is heat treated at the
32
33 second crystallization peak temperature (1344 °C for 2.5 h). To confirm whether the
34
35 Y2S-2 glass ceramic belongs to surface crystallization or that the rate of crystallization
36
37 is too fast at second crystallization peak temperature leading to complete crystallization,
38
39 the Y2S-3 sample is annealed only at 1344 °C for 5 min without at 920 °C for 1 h, as
40
41 shown in Fig. 6 (d), it is still overall crystallization even though such short heat
42
43
44
45
46
47
48
49
50
51
52
53
54
55
56
57
58
59
60
61
62
63
64
65

1 treatment duration. Besides, comparing the profile photos of all glass ceramics (Fig.6),
2
3
4 it is found that Y2S glass is the most easily crystallized which is well in agreement with
5
6
7 DSC results because of the highest enthalpy of Y2S glass. Therefore, it is really
8
9
10 interesting for Y2S glass how to control glass ceramics microstructure (surface or
11
12
13 overall crystallization) and precipitated crystals (γ -Y₂Si₂O₇ or Y_{4.67}(SiO₄)₃O crystals).
14
15

16 By the DSC analysis and crystallization behavior for SPG (Y2S) and NSPG (Y, M
17
18 and YMS) samples, there is an exothermic peak for the NSPG samples caused by phase
19
20
21 separation in DSC curve, phase separation of the NSPG samples is occurred when it is
22
23
24 heat treated at this temperature (Tx), which lead to the obvious crystallization of NSPG
25
26
27 samples as the heat treating temperature is elevated to the crystallization peak
28
29
30 temperature (Tc). In the case of SPG sample, there are two exothermic peaks in DSC
31
32
33 curve, and no phase separation is observed, while Y_{4.67}(SiO₄)₃O crystal is precipitated
34
35
36 along the sample surface when SPG sample is heat treated at the first exothermic peak
37
38
39 temperature. Main γ -Y₂Si₂O₇ and little Y_{4.67}(SiO₄)₃O crystals are precipitated from the
40
41
42 SPG sample when SPG sample is annealed at second exothermic peak temperature, and
43
44
45 it is the overall crystallization even though very short heat treatment duration (5min) at
46
47
48 the second exothermic peak temperature.
49

50 51 **3.3. Structure analysis**

52 The FT-IR spectra of the parent glasses in the wavenumber range of 400-1400 cm⁻¹,
53
54
55 400-650 cm⁻¹ and 850-1350 cm⁻¹ are showed in Fig. 7 (a), (b) and (c), respectively. The
56
57
58
59
60
61
62
63
64
65

1 band located in the range of 448-465 cm^{-1} is assigned to bending vibrations of the T-O-T
2
3
4 (T=Si or Al) bonds, and another band in the range of 470-510 cm^{-1} is assigned to
5
6
7 Si-O-Si bending vibration mode [5,18,22] and overlapped with the former. The
8
9
10 overlapped bands at 600-750 cm^{-1} are connected with Si-O-(Si, Al) symmetric
11
12
13 stretching vibrations between the tetrahedral. The absorption band centered at 685 cm^{-1}
14
15
16 is due to the bending Si-O-Al vibrations as well as to the stretching vibrations of the Al-
17
18
19 O bond in the alumino-oxygen tetrahedral, and the shoulder at about 620 cm^{-1} definitely
20
21
22 should be associated with the silicon-aluminum-oxygen ring vibrations [23-26]. The
23
24
25 absorption band at about 760-800 cm^{-1} represents Si-O-Si symmetric stretching
26
27
28 vibration, but a contribution to this absorption band could arise also from
29
30
31 tetra-coordinated aluminium [5,27,28]. Besides, the spectral range of 500-600 cm^{-1} is
32
33
34 expected to be assigned to Y-O stretching vibration [27]. It can be seen from Fig. 7 (b)
35
36
37 that Y and Y2S glasses have lower absorption intensity than the samples of M and YMS
38
39
40 at nearby 470 cm^{-1} band belonging to Si-O-Si bending vibration, so Y and Y2S have
41
42
43 more non-bridging oxygen and weak network connectivity. Moreover, this band that
44
45
46 moved toward higher wavenumber is due to the fact that Y and Y2S have more strong
47
48
49 Y-O bonds resulting from high Y/Si ratio.

50
51 The intense absorption band in the range of 850-1200 cm^{-1} is the asymmetric
52
53
54 stretching vibration of Si-O-Si bonds in the SiO_4 tetrahedron with different numbers of
55
56
57 bridging oxygen atoms [15,29,30]. This band comprises the unit Q^n standing for a
58
59
60
61
62
63
64
65

1 silicon tetrahedron containing n bridging oxygen (BO), namely, Q^0 (SiO_4^{4-} monomer),
2
3
4 Q^1 ($Si_2O_7^{6-}$ dimer), Q^2 (SiO_3^{2-} chain), Q^3 ($Si_2O_5^{2-}$ sheet), Q^4 (SiO_2
5
6
7 three-dimensional network) [31]. Besides, this band can be also interpreted as vibration
8
9
10 in structural units associated with vibration of aluminosilicate ring formed by Si and Al
11
12
13 tetrahedra [23-26]. It can be observed from Fig. 7 (c) that Y and Y2S glasses have
14
15
16 higher absorption intensity at nearby 920 cm^{-1} band and lower absorption intensity at
17
18
19 nearby 1080 cm^{-1} band than the samples of M and YMS. For more precise quantitative
20
21
22 analysis, the absorption band attributed to the Si-O-Si asymmetric stretching vibration is
23
24
25 deconvoluted by Gaussian model in Origin 8, the bands positions, widths and intensities
26
27
28 are independent and unconstraint variables in curve fitting procedure. The R square for
29
30
31 all fitting data are more than 99.6 %, and the fitting results of four samples are given in
32
33
34 Fig. 8. Table 3 gives the frequencies, areas and area% and these bands at near 900 cm^{-1} ,
35
36
37 960 cm^{-1} , 1095 cm^{-1} and 1190 cm^{-1} respectively contributed to Q^1 , Q^2 , Q^3 and Q^4 .
38
39 Shakeri et al. [18] and Mahdy et al. [5] reported that some little changes such as
40
41
42 reduction of bands absorption intensity in $CaO-MgO-Al_2O_3-SiO_2$ system or
43
44
45 $Li_2O-Al_2O_3-SiO_2$ system by increasing of Y_2O_3 content illustrated the prominent role of
46
47
48 Y^{3+} ions as network former in the glass. Noritaka Saito et al. [32] suggested Y^{3+} ions
49
50
51 exist as network modifier in the glass according to the results of viscosity of
52
53
54 Y-Al-Si-O-N glass melts and Vickers hardness of oxynitride glasses. However, the Y^{3+}
55
56
57 ionic radius is larger than Al^{3+} ionic radius [33], so Y^{3+} cations have a priority to occupy
58
59
60
61
62
63
64
65

1 octahedral voids as network modifier. As the Y/Si ratio (shown in Table 1) increases, the
 2
 3
 4 bridging oxygen of glasses is decreased, and so Y^{3+} ions serve as network modifier
 5
 6
 7 existing in the studied glasses and Y_2O_3 provides free oxygen in yttrium aluminosilicate
 8
 9
 10 glass system.

11
 12
 13 Our group previously calculated the average number of NBO per tetrahedron
 14
 15
 16 (NBO/tetrahedron) and average number of bridging corners per tetrahedron
 17
 18
 19 (bridges/tetrahedron) by the deconvoluted Raman spectra of high frequency region
 20
 21
 22 attributed to the Si-O stretching vibration of $[SiO_4]$ tetrahedron structural units Q^n with
 23
 24
 25 0-4 bridged oxygens for base and rare earth oxides doped soda-lime-silicate glasses
 26
 27
 28 [31,34-35]. The expressions are given as follows.

$$30$$

$$31 \quad X_{NBO/T} = \sum_{i=1}^3 X_i n_i$$

$$32$$

$$33$$

$$34$$

$$35 \quad \frac{NBO}{tetrahedron} = \frac{\sum Q^n (4-n)}{[Si + Al]}$$

$$36$$

$$37$$

$$38$$

$$39 \quad \frac{bridges}{tetrahedron} = \frac{\sum Q^n n}{[Si + Al]}$$

$$40$$

$$41$$

$$42$$

43 where X_i is the mole fraction of SiO_4 units with n_i non-bridging oxygen per silicon. The
 44
 45
 46 deconvoluted infrared spectrum of Si-O-Si asymmetric stretching vibration is analyzed
 47
 48
 49 by the above calculation method to study the effect of chemical composition of YAS
 50
 51
 52 glass on structure and crystallization behavior. The fraction and content of structure
 53
 54
 55 units Q^n , fraction of non-bridging oxygen, average number of NBO per tetrahedron and
 56
 57
 58 average number of bridging corners per tetrahedron for the investigated glasses are
 59
 60
 61
 62
 63
 64
 65

1
2 summarized in Table 4. It can be observed that as the Y/Si ratio increases in chemical
3
4 composition of glass, Q^1 and Q^2 are increased, Q^3 and Q^4 are decreased, and the
5
6 nonbridging oxygen and the bridge per tetrahedron of glasses are increased and
7
8 decreased respectively, as a result, the whole glass structure connectivity is weakened,
9
10 which is in agreement with the variation trend of glass transition temperature (as shown
11
12 in table 1), indicating that increasement of Y/Si ratio in YAS glass makes more
13
14 nonbridging oxygens in glass and glass structure more open, resulting in glass transition
15
16 temperature decrease. And according to the report of other scholars [14], $Y_{4.67}(SiO_4)_3O$
17
18 unit cell is made up of Y^{3+} and silicon-oxygen tetrahedron and the $y-Y_2Si_2O_7$ unit cell
19
20 consists of Y^{3+} and $[Si_2O_7]^{6-}$, $[Si_2O_7]^{6-}$ is formed by a bridging oxygen connecting two
21
22 silicon-oxygen tetrahedron. Thereby, more Q^1 and Q^2 content in glass structure is
23
24 advantageous to crystallize $Y_{4.67}(SiO_4)_3O$ and $y-Y_2Si_2O_7$ crystal. Consequently, the Y
25
26 and Y2S glasses is easier to precipitate $Y_{4.67}(SiO_4)_3O$ or $y-Y_2Si_2O_7$ single or main
27
28 crystal.
29
30
31
32
33
34
35
36
37
38
39
40
41

42 **4. Conclusion**

43
44
45 Crystallization behavior and structure analysis of YAS glasses have been studied in
46
47 this work. The glass chemical composition locating at the higher temperature of liquidus
48
49 surface in YAS phase diagram has lower peak crystallization temperature due to the
50
51 higher enthalpy in glass structure. The crystallization mechanism for NSPG glasses (Y,
52
53 M and YMS) and the SPG glass (Y2S heat treated at the first exothermic peak
54
55
56
57
58
59
60
61
62
63
64
65

1
2 temperature) all belong to surface crystallization, while SPG glass (Y2S heat treated at
3
4 the second exothermic peak temperature) belong to overall crystallization, and the
5
6 stoichiometric parent glass having the same stoichiometric ratio with the precipitated
7
8 crystal, is more easily crystallization than non-stoichiometric parent glass composition.
9
10
11 Besides, NSPG glasses (Y, M and YMS) is observed occurrence of phase separation
12
13 when it is annealed at the exothermic peak temperature between glass transition
14
15 temperature and crystallization peak temperature, and their crystallization behavior at
16
17 crystallization peak temperature is caused by the phase separation. Y-2 and Y2S-2 glass
18
19 ceramics are observed mainly existing γ - $Y_2Si_2O_7$ crystal, Y2S-1 glass ceramic is
20
21 precipitated only $Y_{4.67}(SiO_4)_3O$ apatite. Y and Y2S glasses are easier to precipitate
22
23 $Y_{4.67}(SiO_4)_3O$ or γ - $Y_2Si_2O_7$ single or mainly crystal, which mainly because more Q^1 and
24
25 Q^2 content in glass structure is advantageous to crystallize $Y_{4.67}(SiO_4)_3O$ and γ - $Y_2Si_2O_7$
26
27 crystal in view of crystal structure point. Consequently, this work has a technical
28
29 guiding role in controlling the crystallization process (overall and surface crystallization)
30
31 and the types of precipitated crystals of YAS glass for different application potentials.
32
33
34
35
36
37
38
39
40
41
42
43
44

45 **Acknowledgements**

46
47 This project is financially supported by National Natural Science Foundation of
48
49 China (51974168, 51662033 and 51362019), Natural Science Foundation of the Inner
50
51 Mongolia Autonomous Region (2016JQ05).
52
53
54
55
56
57
58
59
60
61
62
63
64
65

1
2 **Author Information**
3

4
5 *Corresponding author:
6

7 Pro. Mitang Wang: E-mail: btwmt@126.com, Tel: +86-15848255894
8
9

10
11
12
13 **References**
14

15 [1] S. Tanabe, K. Hirao, N. Soga, Elastic properties and molar volume of rare-earth
16 aluminosilicate glasses, J. Am. Ceram. Soc. 75 (2010) 503-506,
17
18 doi:10.1111/j.1151-2916.1992.tb07833.x.
19

20
21
22 [2] S. Hampshire, M. J. Pomeroy, Grain boundary glasses in silicon nitride: a review of
23 chemistry, properties and crystallisation, J. Eur. Ceram. Soc. 32 (2012) 1925-1932,
24
25 doi:<https://doi.org/10.1016/j.jeurceramsoc.2011.12.023>.
26
27

28
29 [3] M. Herrmann, W. Lippmann, A. Hurtado, Y₂O₃-Al₂O₃-SiO₂-based glass-ceramic
30 fillers for the laser-supported joining of SiC, J. Eur. Ceram. Soc. 34 (2014) 1935-1948,
31
32 doi:<https://doi.org/10.1016/j.jeurceramsoc.2014.01.019>.
33
34

35
36 [4] Y. J. Lin, S. H. Tu, Joining of mullite ceramics with yttrium aluminosilicate glass
37 interlayers, Ceram. Int. 35 (2009) 1311-1315.
38
39

40
41 [5] E. A. Mahdy, S. Ibrahim, Influence of Y₂O₃ on the structure and properties of
42 calcium magnesium aluminosilicate glasses, J. Mol. Struct. 1027 (2012) 81-86,
43
44 doi:<https://doi.org/10.1016/j.molstruc.2012.05.055>.
45
46
47

48
49 [6] E. M. Erbe, D. E. Day, Chemical durability of Y₂O₃-Al₂O₃-SiO₂ glasses for the in
50 vivo delivery of beta radiation, J. Biomed. Mater. Res. A 27 (1993) 1301,
51
52 doi:10.1002/jbm.820271010.
53
54

55
56 [7] M. Kawashita, R. Shineha, H. M. Kim, T. Kokubo, Y. Inoue, N. Araki, Y. Nagata, M.
57
58
59
60
61
62
63
64
65

1 Hiraoka, Y. Sawada, Preparation of ceramic microspheres for in situ radiotherapy of
2 deep-seated cancer, *Biomaterials* 24 (2003) 2955-2963, doi:
3
4 10.1016/S0142-9612(03)00094-2.
5
6

7
8 [8] A. Domanická, R. Klement, A. Prnová, K. Bodišová, D. Galusek, Luminescent
9 rare-earth ions doped $\text{Al}_2\text{O}_3\text{-Y}_2\text{O}_3\text{-SiO}_2$ glass microspheres prepared by flame synthesis,
10
11 *Ceram. Int.* 40 (2014) 6005-6012, doi:<https://doi.org/10.1016/j.ceramint.2013.11.049>.
12
13

14 [9] N. Sadiki, J. P. Coutures, C. Fillet, J. L. Dussossoy, Crystallization of lanthanum and
15 yttrium aluminosilicate glasses, *J. Nucl. Mater.* 348 (2006) 70-78,
16
17 doi:<https://doi.org/10.1016/j.jnucmat.2005.09.003>.
18
19

20 [10] A. V. Kir'Yanov, A. Halder, Y. O. Barmenkov, S. Das, A. Dhar, S. K. Bhadra, V. V.
21 Koltashev, V. G. Plotnichenko, M. C. Paul, Distribution of bismuth and bismuth-related
22 centers in core area of $\text{Y-Al-SiO}_2\text{: Bi}$ fibers, *J. Lightwave Technol.* 33 (2015)
23
24 3649-3659, doi:10.1109/JLT.2015.2449084.
25
26

27 [11] A. V. Kir'Yanov, D. Dutta, Y. O. Barmenkov, S. Das, A. Dhar, V. V. Koltashev, V.
28 G. Plotnichenko, M. C. Paul, Basic and peculiar properties of chromium-magnesium
29 Co-doped YAS-based optical fibers, *IEEE J. Quantum Elect.* 52 (2016) 1-12,
30
31 doi:10.1109/JQE.2016.2568750.
32
33

34 [12] O. Fabrichnaya, H. J. Seifert, R. Weiland, T. Ludwig, F. Aldinger, A. Navrotsky,
35 Phase equilibria and thermodynamics in the $\text{Y}_2\text{O}_3\text{-Al}_2\text{O}_3\text{-SiO}_2$ system, *Z. Metallkd.* 92
36
37 (2001) 1083-1097.
38
39

40 [13] S. Ahmad, T. Ludwig, M. Herrmann, M. M. Mahmoud, W. Lippmann, H. J. Seifert,
41 Phase evaluation during high temperature long heat treatments in the $\text{Y}_2\text{O}_3\text{-Al}_2\text{O}_3\text{-SiO}_2$
42
43 system, *J. Eur. Ceram. Soc.* 34 (2014) 3835-3840,
44
45 doi:<https://doi.org/10.1016/j.jeurceramsoc.2014.05.025>.
46
47
48
49
50
51
52
53
54
55
56
57
58
59
60
61
62
63
64
65

- 1 [14] Z. Q. Sun, M. S. Li, Y. C. Zhou, Recent progress on synthesis, multi-scale
2 structure, and properties of Y-Si-O oxides, *Int. Mater. Rev.* 59 (2014) 357-383,
3
4
5
6 doi:10.1002/chin.201513295.
7
- 8 [15] W. Zhu, H. Jiang, H. Zhang, Y. Liu, Effect of TiO₂ and CaF₂ on the crystallization
9 behavior of Y₂O₃-Al₂O₃-SiO₂ glass ceramics, *Ceram. Int.* 44 (2018) 6653-6658,
10
11
12
13 doi:10.1016/j.ceramint.2018.01.076.
14
- 15 [16] H. Okudera, Y. Masubuchi, S. Kikkawa, A. Yoshiasa, Structure of oxide
16 ion-conducting lanthanum oxyapatite, La_{9.33}(SiO₄)₆O₂, *Solid State Ionics* 176 (2005)
17
18
19
20
21
22 1473-1478, doi:https://doi.org/10.1016/j.ssi.2005.02.014.
23
- 24 [17] T. Liao, T. Sasaki, S. Suehara, Z. Sun, Position preference and diffusion path of an
25 oxygen ion in apatite-type lanthanum silicate La_{9.33}Si₆O₂₆: a density functional study, *J.*
26
27
28
29
30
31
32
33
34
35
36
37
38
39
40
41
42
43
44
45
46
47
48
49
50
51
52
53
54
55
56
57
58
59
60
61
62
63
64
65
- [18] M. S. Shakeri, M. Rezvani, Optical band gap and spectroscopic study of lithium
alumino silicate glass containing Y³⁺ ions, *Spectrochim. Acta A* 79 (2011) 1920-1925,
doi:https://doi.org/10.1016/j.saa.2011.05.090.
- [19] K. Singh, N. Gupta, O. P. Pandey, Effect of Y₂O₃ on the crystallization behavior of
SiO₂-MgO-B₂O₃-Al₂O₃ glasses, *J. Mater. Sci.* 42 (2007) 6426-6432,
doi:10.1007/s10853-006-1188-z.
- [20] I. A. Bondar, F. Ya. Galakhov, Phase equilibria in the system Y₂O₃-Al₂O₃-SiO₂,
Russ Chem B+ 13 (1964) 1231-1232, doi:10.1007/BF00863139.
- [21] Shelby J E. *Introduction to Glass Science and Technology*, Second ed., Royal
Society of Chemistry, Cambridge, 2005.
- [22] Z. Yang, Q. Lin, S. Lu, Y. He, G. Liao, Y. Ke, Effect of CaO/SiO₂ ratio on the
preparation and crystallization of glass-ceramics from copper slag, *Ceram. Int.*

1 40(2014)7297-7305, doi: 10.1016/j.ceramint.2013.12.071.
2

3 [23] M. Sitarz, W. Mozgawa, M. Handke, Rings in the structure of silicate glasses, J.
4 Mol. Struct. 511-512 (1999) 281-285. doi: 10.1016/S0022-2860(99)00169-6.
5

6 [24] M. Sitarz, The structure of simple silicate glasses in the light of middle infrared
7 spectroscopy studies, J. Non-Cryst. Solids 357 (2011) 1603-1608. doi:
8 10.1016/j.jnoncrysol.2011.01.007.
9

10 [25] M. Sitarz, M. Handke, W. Mozgawa, Identification of silicoxygen rings in SiO₂
11 based on IR spectra, Spectrochim Acta A 56 (2000) 1819-1823. doi:
12 10.1016/S1386-1425(00)00241-9.
13

14 [26] M. Sitarz, M. Handke, W. Mozgawa, E. Galuskin, I. Galuskina, The non-ring
15 cations influence on silicoxygen ring vibrations, J. Mol. Struct. 555 (2000) 357-362.
16 doi: 10.1016/S0022-2860(00)00621-9.
17

18 [27] D. Eniu, S. Simon, Structural properties of melt versus sol-gel derived yttrium
19 aluminosilicate systems, Ceram. Int. 44 (2018) 9581-9584,
20 doi:10.1016/j.ceramint.2018.02.181.
21

22 [28] Y. Li, K. Liang, J. Cao, B. Xu, Spectroscopy and structural state of V⁴⁺ ions in
23 lithium aluminosilicate glass and glass-ceramics, J. Non-Cryst. Solids 356 (2010)
24 502-508, doi:10.1016/j.jnoncrysol.2009.12.018.
25

26 [29] J. Zhao, Y. Lu, J. Kang, Y. Qu, G. A. Khater, S. Li, Y. Wang, Y. Yue, Effect of Y₂O₃
27 and La₂O₃ on structure and dielectric properties of aluminoborosilicate glasses, J.
28 Non-Cryst. Solids 496 (2018) 1-5, doi:10.1016/j.jnoncrysol.2018.05.020.
29

30 [30] F. Pei, H. Guo, P. Li, B. Yan, J. Li, P. Yang, G. Zhu, Influence of low magnesia
31 content on the CaO-Al₂O₃-SiO₂ glass-ceramics: Its crystallization behaviour,
32 microstructure and physical properties, Ceram. Int. 44(2018)20132-20139, doi:
33
34
35
36
37
38
39
40
41
42
43
44
45
46
47
48
49
50
51
52
53
54
55
56
57
58
59
60
61
62
63
64
65

1 10.1016/j.ceramint.2018.07.306.
2

3 [31] M. Wang, J. Cheng, M. Li, F. He, Raman spectra of soda-lime-silicate glass doped
4 with rare earth, *Physica B* 406 (2011) 3865-3869, doi:10.1016/j.physb.2011.07.014.
5

6 [32] N. Saito, K. Kai, S. Furusho, K. Nakashima, K. Mori, Properties of
7 nitrogen-containing yttria-alumina-silica melts and glasses, *J. Am. Ceram. Soc.* 67
8 (2003) 40-46, doi:10.2320/jinstmet1952.67.1_40.
9

10 [33] K. Singh, N. Gupta, O. P. Pandey, Effect of Y_2O_3 on the crystallization behavior of
11 SiO_2 - MgO - B_2O_3 - Al_2O_3 glasses, *J. Mater. Sci.* 42 (2007) 6426-6432,
12 doi:10.1007/s10853-006-1188-z.
13

14 [34] M. Wang, M. Li, J. Cheng, F. He, Z. Liu, Y. Hu, Free volume and structure of
15 Gd_2O_3 and Y_2O_3 co-doped silicate glasses, *J. Non-Cryst. Solids* 379 (2013)145-149, doi:
16 10.1016/j.jnoncrysol.2013.08.003.
17

18 [35] M. Wang, M. Li, J. Cheng, F. He, Structure and viscosity of soda lime silicate
19 glasses with varying Gd_2O_3 content, *J. Mol. Struct.* 1063 (2014) 139-144, doi:
20 10.1016/j.molstruc.2014.01.062.
21
22
23
24
25
26
27
28
29
30
31
32
33
34
35
36
37
38
39
40
41
42
43
44
45
46
47
48
49
50
51
52
53
54
55
56
57
58
59
60
61
62
63
64
65

1 Figure captions
2

3 Fig. 1 The Y_2O_3 - Al_2O_3 - SiO_2 phase diagram. YAM: $Y_4Al_2O_9$; YAP: $YAlO_3$; YAG:
4 $Y_3Al_5O_{12}$; Mull: Mullite; TR: Tridymite; Y, Y2S, M and YMS are the studied glasses in
5
6 this work.
7
8
9

10 Fig. 2 DSC curves of glasses Y, Y2S, M and YMS. T_c is the first crystallization peak
11 temperature; T_{c2} the second crystallization peak temperature; T_x is the temperature
12
13 between glass transition temperature (T_g) and the first crystallization peak temperature.
14
15
16
17

18 Fig. 3 XRD patterns of the heat treated glasses
19

20 Fig. 4 SEM micrographs (a) Y-1, (b) Y-2, (c) Y2S-1, (d) Y2S-2
21
22

23 Fig. 5 EDS results of Si and Y elements in and nearby the phase separation area for Y-1
24
25
26 sample
27

28 Fig. 6 Profile photos of the annealed glasses (a)Y-2, (b) Y2S-1, (c)Y2S-2, (d)Y2S-3, (e)
29
30 M-2, (f) YMS-2, (g) YMS-3
31
32
33
34

35 Fig. 7 IR spectra of the studied parent glass (a) 400 - 1400 cm^{-1} , (b) 400 - 650 cm^{-1} , (c)
36
37 850 - 1350 cm^{-1}
38
39
40

41 Fig. 8 Deconvoluted IR spectrum at 850 - 1300 cm^{-1} of YAS glasses: (a) Y, (b) Y2S, (c)
42
43 M, (d) YMS
44
45
46
47
48
49
50
51
52
53
54
55
56
57
58
59
60
61
62
63
64
65

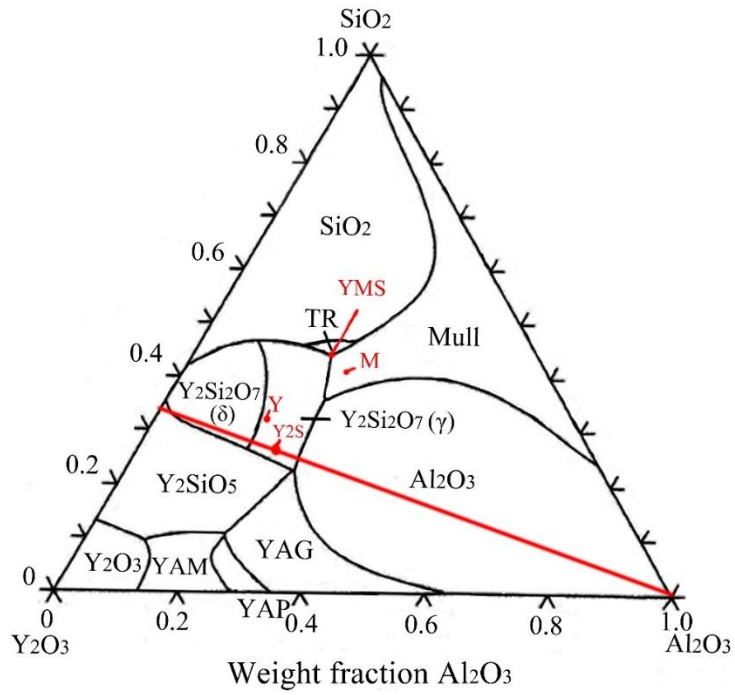


Fig. 1

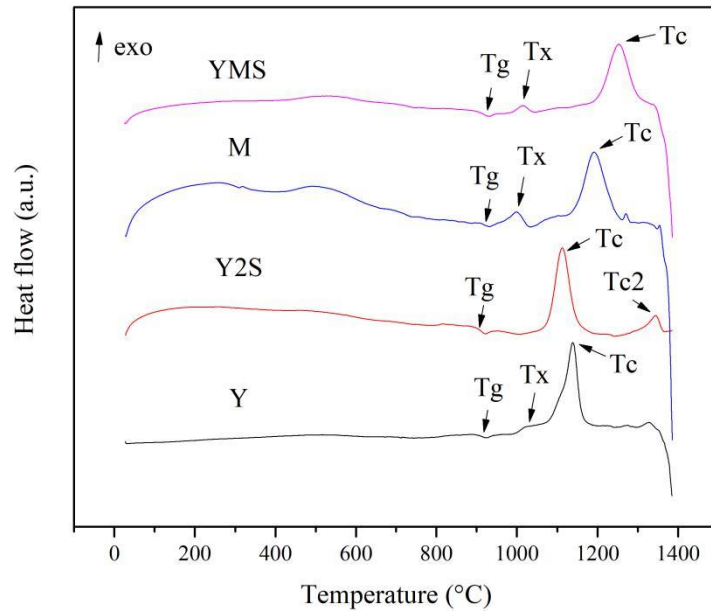


Fig. 2

1
2
3
4
5
6
7
8
9
10
11
12
13
14
15
16
17
18
19
20
21
22
23
24
25
26
27
28
29
30
31
32
33
34
35
36
37
38
39
40
41
42
43
44
45
46
47
48
49
50
51
52
53
54
55
56
57
58
59
60
61
62
63
64
65

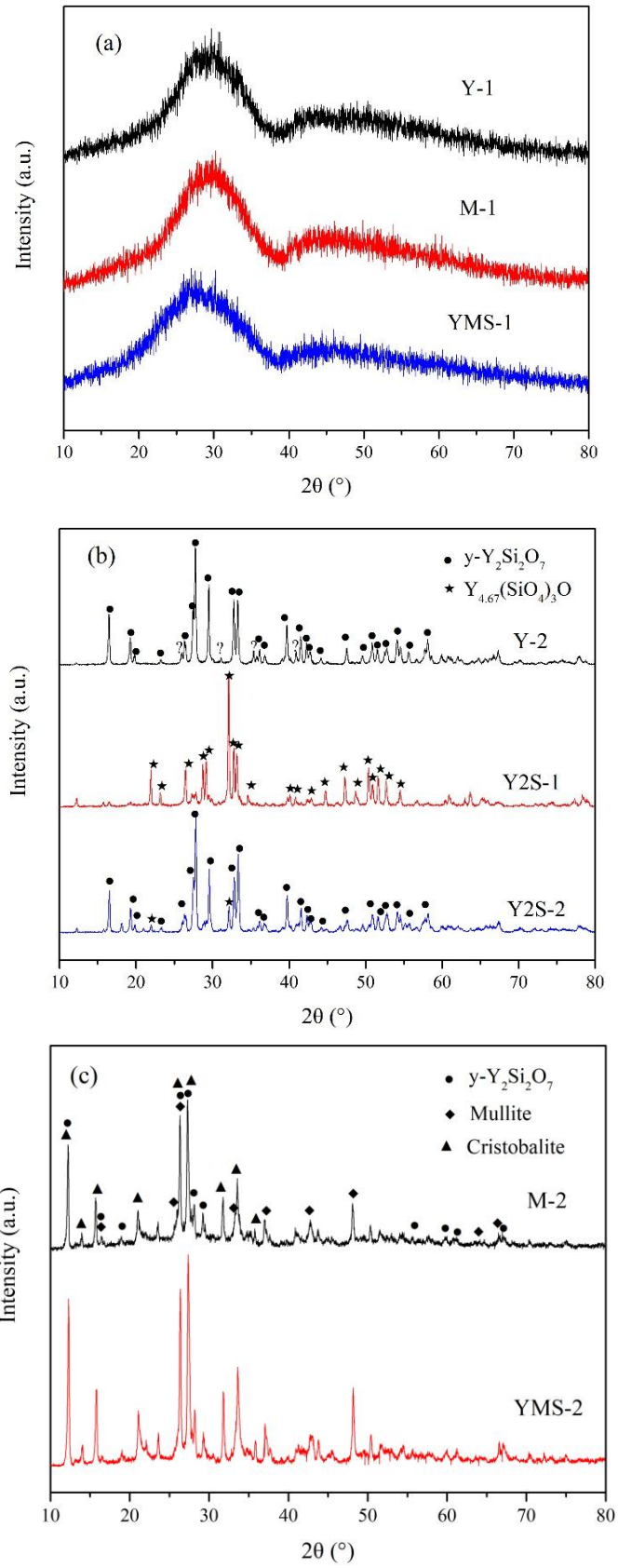


Fig. 3

1
2
3
4
5
6
7
8
9
10
11
12
13
14
15
16
17
18
19
20
21
22
23
24
25
26
27
28
29
30
31
32
33
34
35
36
37
38
39
40
41
42
43
44
45
46
47
48
49
50
51
52
53
54
55
56
57
58
59
60
61
62
63
64
65

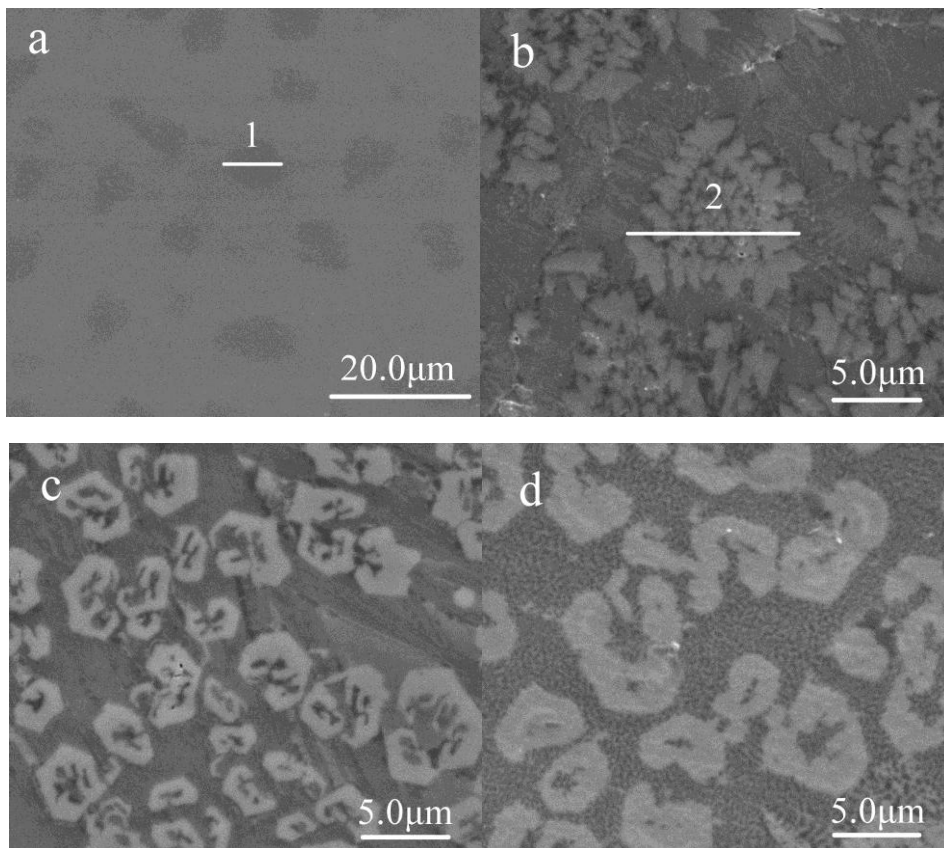


Fig. 4

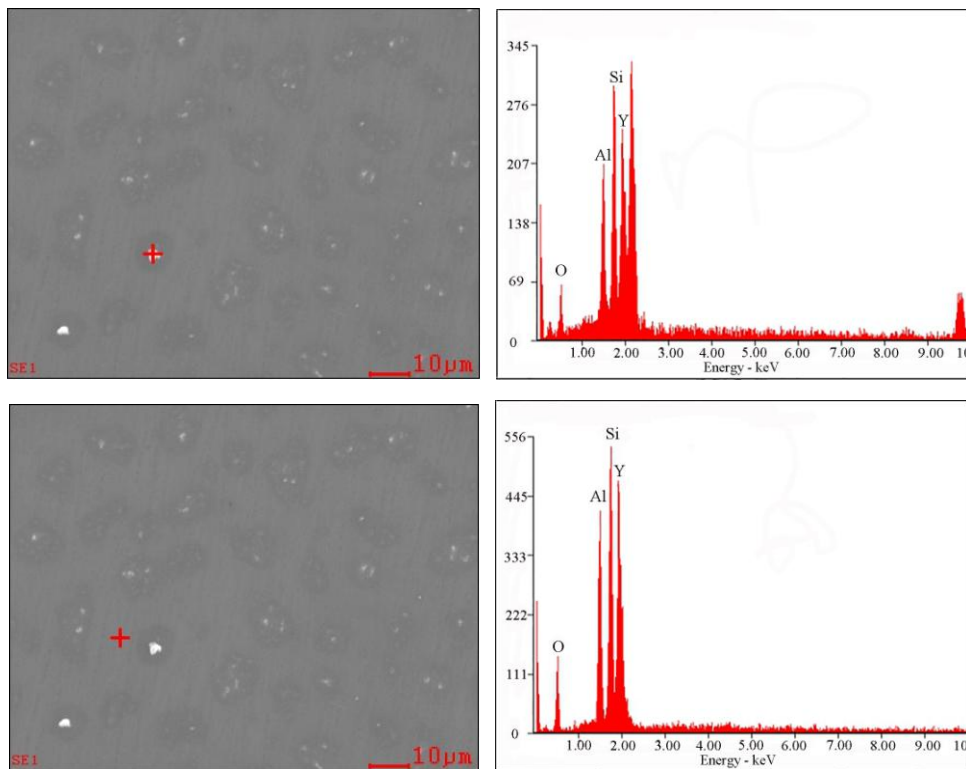


Fig. 5

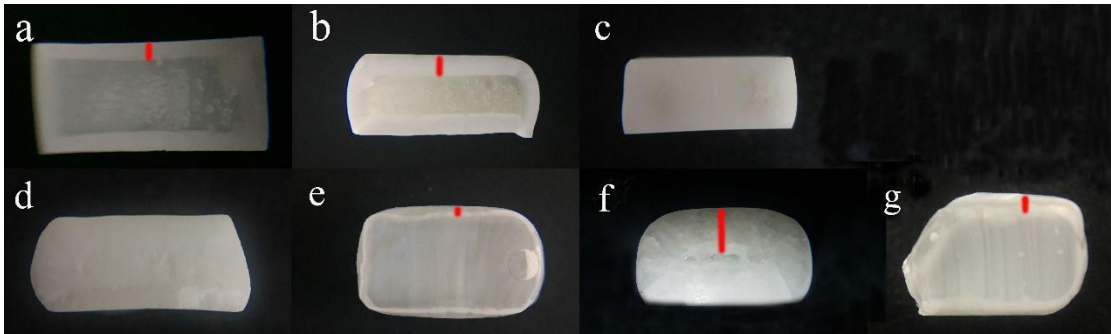


Fig. 6

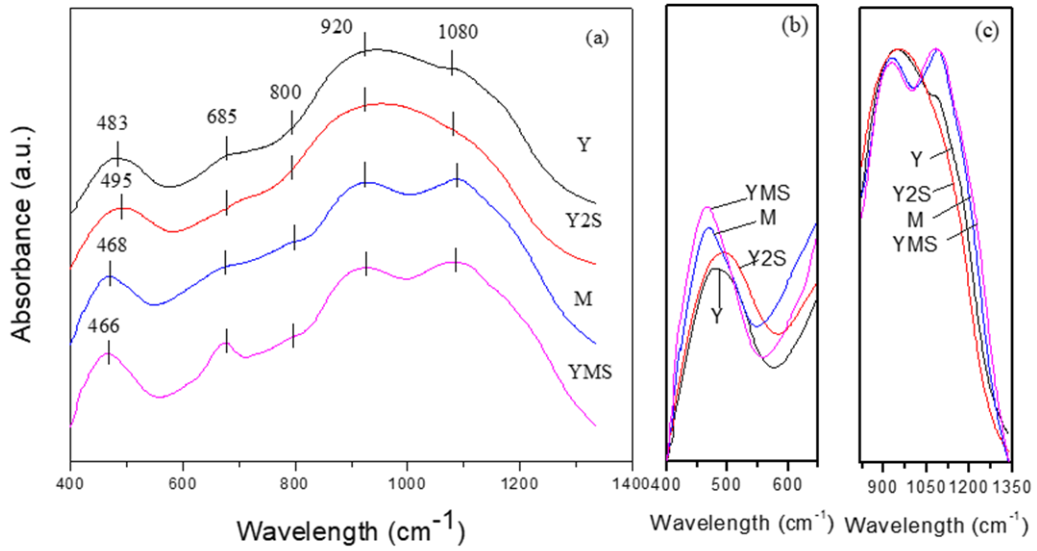


Fig. 7

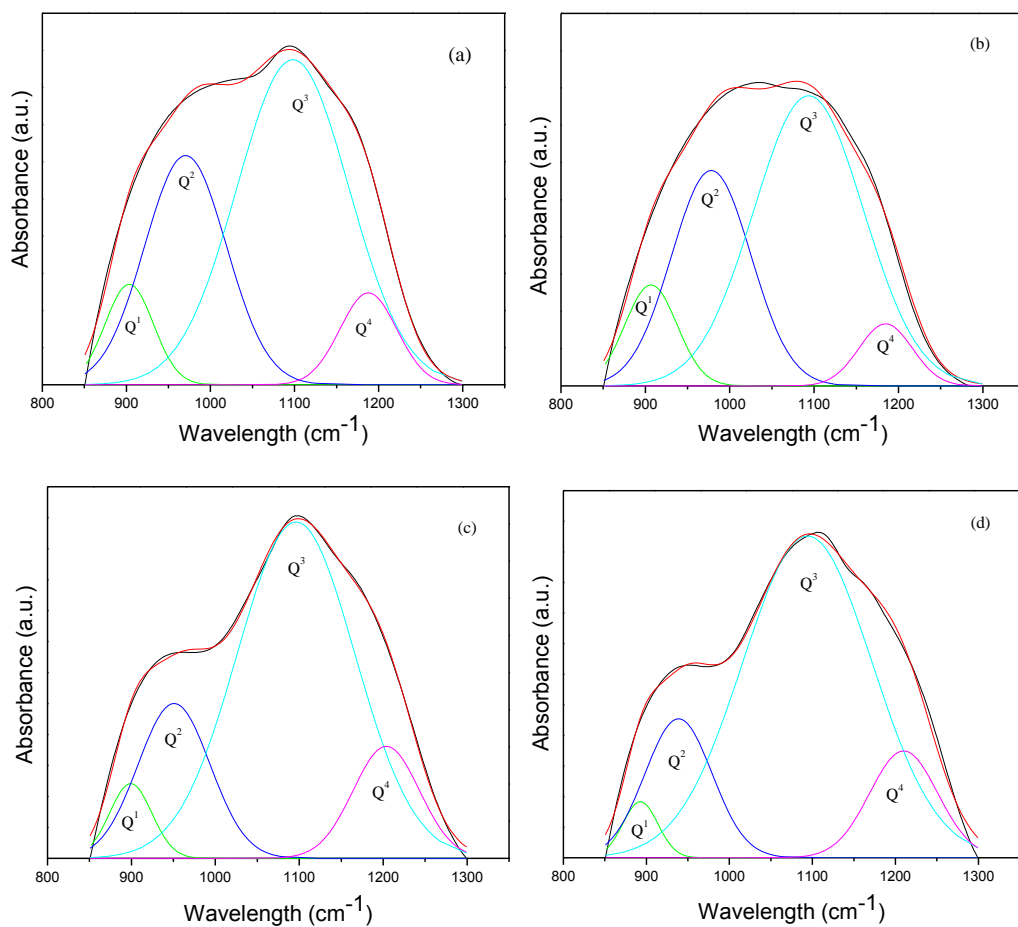


Fig. 8

Table 1. Chemical compositions (mol %), glass transition and crystallization temperatures of glass samples

Sample	Y ₂ O ₃	Al ₂ O ₃	SiO ₂	Y/Si	T _g (°C)	T _x (°C)	T _c (°C)	T _{c2} (°C)
Y	22	19	59	0.74	906	1035	1137	—
Y2S	25	25	50	1.00	905	—	1112	1344
M	11.89	23.17	64.94	0.37	915	999	1191	—
YMS	12.62	19.21	68.17	0.37	913	1015	1253	—

Table 2. Heat treatment schedules and crystallization behavior for glasses

Sample	Annealing(T, t)		Observed phase
Y-1	920 °C, 1 h	1035 °C, 2.5 h	No crystallization
Y-2	920 °C, 1 h	1137 °C, 2.5 h	y-Y ₂ Si ₂ O ₇
Y2S-1	920 °C, 1 h	1112 °C, 2.5 h	Y _{4.67} (SiO ₄) ₃ O
Y2S-2	920 °C, 1 h	1344 °C, 2.5 h	y-Y ₂ Si ₂ O ₇ +(little) Y _{4.67} (SiO ₄) ₃ O
Y2S-3	920 °C, 0 h	1344 °C, 5 min	y-Y ₂ Si ₂ O ₇ +(little) Y _{4.67} (SiO ₄) ₃ O
M-1	920 °C, 1 h	999 °C, 2.5 h	No crystallization
M-2	920 °C, 1 h	1191 °C, 2.5 h	y-Y ₂ Si ₂ O ₇ + mullite + cristobalite
YMS-1	920 °C, 1 h	1015 °C, 2.5 h	No crystallization
YMS-2	920 °C, 1 h	1253 °C, 2.5 h	y-Y ₂ Si ₂ O ₇ + mullite + cristobalite
YMS-3	920 °C, 1 h	1253 °C, 0.5 h	y-Y ₂ Si ₂ O ₇ + mullite + cristobalite

y-Y₂Si₂O₇ (JCPDS-22-1103); Y_{4.67}(SiO₄)₃O (JCPDS-30-1457); mullite (JCPDS-02-0431); cristobalite (JCPDS-03-0276).

1
2
3
4
5
6
7
8
9
10
11
12
13
14
15
16
17
18
19
20
21
22
23
24
25
26
27
28
29
30
31
32
33
34
35
36
37
38
39
40
41
42
43
44
45
46
47
48
49
50
51
52
53
54
55
56
57
58
59
60
61
62
63
64
65

Table 3 Frequencies (V/cm^{-1}), areas (A) and area % (A%) of IR bands obtained from the deconvolution fitting

	Y	Y2S	M	YMS
V1	903	907	899	893
V2	970	978	951	939
V3	1098	1094	1096	1094
V4	1188	1185	1204	1210
A1	9.41	10.14	7.42	4.74
A2	37.32	33.96	26.62	22.65
A3	72.98	63.37	95.50	102.25
A4	10.48	6.61	17.78	17.65
A1%	7.22	8.88	5.04	3.21
A2%	28.66	29.77	18.07	15.38
A3%	56.06	55.55	64.82	69.42
A4%	8.05	5.79	12.07	11.98

Table 4 Fraction ($X^n\%$) and content ($Q^n/\%$) of structure units, average number of NBO per tetrahedron and average number of bridging corners per tetrahedron

	Y	Y2S	M	YMS
$X^1\%$	8.30	10.21	5.80	3.69
$X^2\%$	29.23	30.37	18.43	15.69
$X^3\%$	58.30	57.77	67.41	72.20
$X^4\%$	4.16	1.65	8.36	8.42
Q^1	8.05	10.21	6.45	3.94
Q^2	28.36	30.37	20.51	16.72
Q^3	56.55	57.77	75.02	76.95
Q^4	2.46	0.83	5.43	5.74
NBO/tetrahedron	1.42	1.49	1.22	1.15
bridges/tetrahedron	2.58	2.51	2.78	2.85

Figure captions

1
2 Fig. 1 The Y_2O_3 - Al_2O_3 - SiO_2 phase diagram. YAM: $Y_4Al_2O_9$; YAP: $YAlO_3$; YAG:
3
4 $Y_3Al_5O_{12}$; Mull: Mullite; TR: Tridymite; Y, Y2S, M and YMS are the studied glasses
5
6 in this work.
7

8
9 Fig. 2 DSC curves of glasses Y, Y2S, M and YMS. T_c is the first crystallization peak
10
11 temperature; T_{c2} the second crystallization peak temperature; T_x is the temperature
12
13 between glass transition temperature (T_g) and the first crystallization peak
14
15 temperature.
16
17

18
19 Fig. 3 XRD patterns of the heat treated glasses
20

21
22 Fig. 4 SEM micrographs (a) Y-1, (b) Y-2, (c) Y2S-1, (d) Y2S-2
23

24
25 Fig. 5 EDS results of Si and Y elements in and nearby the phase separation area for
26
27 Y-1 sample
28

29
30 Fig. 6 Profile photos of the annealed glasses (a)Y-2, (b) Y2S-1, (c)Y2S-2, (d)Y2S-3,
31
32 (e) M-2, (f) YMS-2, (g) YMS-3
33

34
35 Fig. 7 IR spectra of the studied parent glass (a) 400 - 1400 cm^{-1} , (b) 400 - 650 cm^{-1} , (c)
36
37 850 - 1350 cm^{-1}
38

39
40 Fig. 8 Deconvoluted IR spectrum at 850 - 1300 cm^{-1} of YAS glasses: (a) Y, (b) Y2S, (c)
41
42 M, (d) YMS
43
44
45
46
47
48
49
50
51
52
53
54
55
56
57
58
59
60
61
62
63
64
65